Mechanisms of enhanced thermal stability of polarization in lead-free $(Bi_{1/2}Na_{1/2})_{0.94}Ba_{0.06}TiO_3$/ZnO ceramic composites

Zhongming Fan,[1] Lin Zhou,[2,*] Tae-Hoon Kim,[2] Ji Zhang,[3] Shan-Tao Zhang,[3] and Xiaoli Tan[1,*]
[1]*Department of Materials Science and Engineering, Iowa State University, Ames, Iowa 50011, USA*
[2]*Ames Laboratory, United States Department of Energy, Ames, Iowa 50011, USA*
[3]*National Laboratory of Solid State Microstructures and Department of Materials Science and Engineering, Nanjing University, Nanjing 210093, China*

(Received 21 October 2018; published 6 February 2019)

$(Bi_{1/2}Na_{1/2})TiO_3$-based solid solutions, one of the major systems of lead-free piezoelectric ceramics, exhibit a low thermal depolarization temperature ($T_d \sim 100\,^{\circ}C$). It was reported that by incorporating 30 mol% ZnO particles to form a ceramic composite of $(Bi_{1/2}Na_{1/2})_{0.94}Ba_{0.06}TiO_3$/ZnO, the depolarization process can be shifted up to ~250 °C. In the present work, a variety of advanced transmission electron microscopy techniques, including *in situ* heating, annular bright-field, high-angle annular dark-field, geometric phase analysis, energy-dispersive spectrum and electron energy-loss spectroscopy, are employed to investigate the underlying mechanisms for the enhanced thermal stability of polarization in the composite. It is found that the abrupt depolarization in $(Bi_{1/2}Na_{1/2})_{0.94}Ba_{0.06}TiO_3$ at T_d becomes diffused over a wide temperature window up to the temperature at maximum dielectric constant (T_m) under the combined actions of the incorporation of Zn into the perovskite lattice, the presence of residual stresses, and the pinning effect on micron-sized domains provided by ZnO particles.

DOI: 10.1103/PhysRevMaterials.3.024402

I. INTRODUCTION

Lead-free ceramics have been the worldwide focus for research in the piezoelectrics community over the past 15 years, motivated by the search for replacement of lead-containing ceramics [1], which are health and environmentally unfriendly. According to their chemical compositions, lead-free piezoceramics are classified into three groups, $BaTiO_3$-based, $(K_{1-x}Na_x)NbO_3$-based, and $(Bi_{1/2}Na_{1/2})TiO_3$-based [2]. Each of these groups possesses specific advantages and shortcomings in comparison with the market-dominating $Pb(Zr_{1-x}Ti_x)O_3$ ceramics. Generally speaking, $BaTiO_3$-based ceramics exhibit outstanding small signal piezoelectric properties (e.g., $d_{33} > 600\,pC/N$), while their working temperature is quite limited due to their low Curie point ($T_c \sim 100\,^{\circ}C$) [3–5]. Modified $(K_{1-x}Na_x)NbO_3$ compositions can achieve values of d_{33} comparable to $Pb(Zr_{1-x}Ti_x)O_3$ and have a moderate Curie point ($T_c > 200\,^{\circ}C$), despite concerns on processing and reproducibility [6–8]. $(Bi_{1/2}Na_{1/2})TiO_3$-based polycrystalline ceramics show a mediocre d_{33} but are capable of developing giant electrostrains [9,10]. However, they suffer from the restriction in working temperature as well. For example, the prototypical $(Bi_{1/2}Na_{1/2})_{0.94}Ba_{0.06}TiO_3$ (BNBT6) undergoes a thermal depolarization at the T_d about 100 °C, above which the micron-sized ferroelectric domains and the associated piezoelectricity vanish [11,12]. The thermal depolarization in $(Bi_{1/2}Na_{1/2})TiO_3$-based ceramics is a manifestation of their complex phase transitions, most of which are still not fully understood.

Massive efforts have been invested in overcoming the shortcomings without sacrificing the advantages in these lead-free composition systems. Recently, we reported a method to eliminate the thermal depolarization in BNBT6, which is to form composites with ZnO particles (BNBT6/0.3ZnO) [13]. A "space charge" model was hypothesized to explain the influence of ZnO particle on T_d: the poling-induced micron-sized ferroelectric domains in BNBT6 are stabilized by charges in the ZnO particles, so that the depolarization of the ferroelectric phase can be significantly delayed. Following the initial work, various research groups have attempted to reproduce the BNBT6/ZnO composites and offered two new interpretations. Riemer *et al.* suggested the "stress field" model: the difference in thermal expansion coefficients of BNBT6 and ZnO leads to compressive stresses in the BNBT6 matrix when cooling down from the sintering temperature, hence the stress-induced relaxor → ferroelectric phase transition takes place in BNBT6 [14]. Mahajan *et al.*, on the other hand, proposed that the increase in T_d of BNBT6/ZnO is essentially a result of Zn incorporation into the BNBT6 lattice that stabilizes the ferroelectric phases to a higher temperature, which is the "Zn doping" model [15].

Despite the plausibility of all three models, none of them have been unambiguously corroborated. In the present work, advanced transmission electron microscopy (TEM) techniques are utilized to unravel the exact mechanisms of the absence of the low temperature thermal depolarization at T_d in the piezoelectric BNBT6/0.3ZnO composite.

*Authors to whom correspondence should be addressed: linzhou@ameslab.gov; xtan@iastate.edu

II. EXPERIMENTAL

Sample preparation. Single phase BNBT6 was prepared first. Stoichiometric Bi_2O_3 (99.8%), $BaCO_3$ (99.0%), Na_2CO_3 (99.8%), and TiO_2 (99.0%, all from Alfa Aesar), were weighed and ball milled in ethanol for 24 h. The dried slurries were calcined at 900 °C for 3 h, ground manually for 0.5 h, ball milled again in ethanol for 24 h, followed by a drying process. The powders were sintered in covered alumina crucibles at 1100 °C for 3 h.

To fabricate the BNBT6/0.3ZnO composite, the sintered single phase BNBT6 was first ground into powder manually for 1 h. Afterward, both the prepared BNBT6 powder and the commercial ZnO nanoparticles with the size of 25 nm (PlasmaChem, Germany) were weighed according to the formula. The mixture was ball milled again in ethanol for 24 h, dried and subsequently pressed into green disks with a diameter of 10 mm under 40 MPa. Sintering was carried out in covered alumina crucibles at 1050 °C for 1 h with a ramp rate of 9 °C min^{-1}.

Electrical properties measurement. The disk samples with a diameter of ~8.5 mm and a thickness of ~0.5 mm were electroded with a thin layer of silver paste fired at 550 °C for 30 min. Dielectric constant (ε_r) and loss tangent (tanδ) were measured using an impedance analyzer (HP4294A) at 100 kHz in a temperature range from 30 to 320 °C on poled samples.

Electron Microscopy. An overall microstructure and element distribution were analyzed by SEM (FEI Helios NanoLab DualBeam). For TEM experiments, as-sintered ceramic pellets were mechanically ground and polished down to 120-μm thick, and then ultrasonically cut into disks with a diameter of 3 mm. After mechanical dimpling and polishing, the disks were annealed at 350 °C for 0.5 h and Ar-ion milled to perforation. The *in situ* heating tests were performed on a TEM of FEI Tecnai G2-F20. The detailed morphology, structure and element characterizations were performed on an aberration-corrected S/TEM (FEI Titan Themis).

III. RESULTS AND DISCUSSION

A. Thermal depolarization at T_d: Delayed or diffused?

There are multiple ways to determine the depolarization temperature in $(Bi_{1/2}Na_{1/2})TiO_3$-based piezoceramics, among which the anomaly in dielectric permittivity is most commonly used [16]. The temperature dependent dielectric constant (ε_r) and loss tangent (tanδ) measured in poled BNBT6/0.3ZnO composite and single phase BNBT6 are compared in Fig. 1. Single phase BNBT6 shows a T_d around 115 °C, manifested by the steep increase of ε_r and a raised plateau between 120 and 140 °C in tanδ. In contrast, ε_r and tanδ increase continuously until T_m in the BNBT6/0.3ZnO composite. It should be noted that the difference between T_m and the temperature of the tanδ peak is typical for relaxor ferroelectrics [17].

There could be two interpretations of the absence of T_d in dielectric curves of BNBT6/0.3ZnO. The first possibility is that T_d is so much delayed that it merges with T_m. The other possible scenario is that the thermal depolarization becomes diffused and spreads over the temperature window

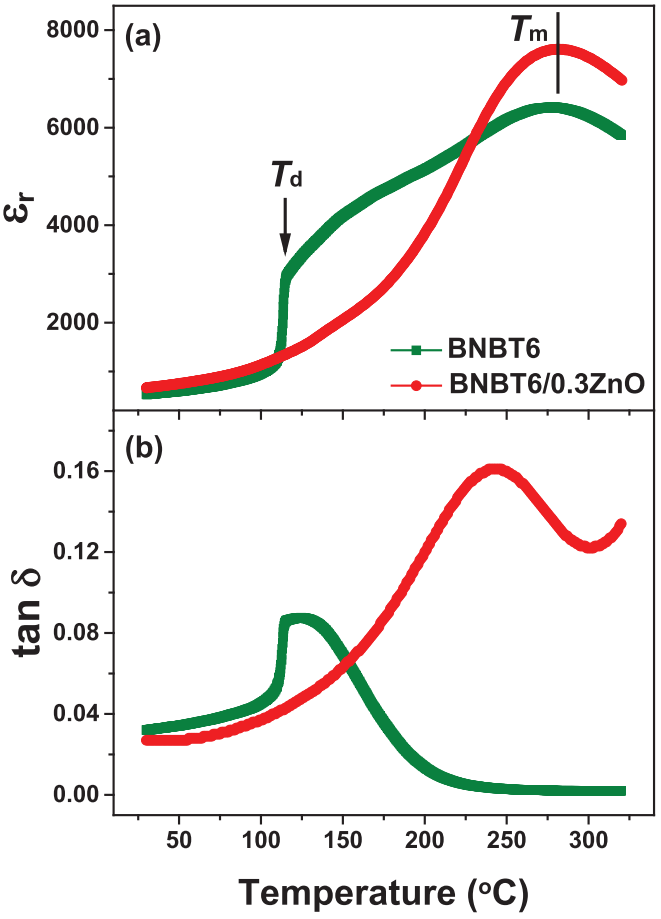

FIG. 1. Temperature dependent (a) dielectric constant and (b) loss tangent measured at 100 kHz on the single phase BNBT6 ceramic and the BNBT6/0.3ZnO composite.

of $T_d \sim T_m$. Owing to the capability of tracking the evolution of microstructure with temperature, *in situ* heating TEM should be able to provide direct evidences to discern these two possible interpretations [18]. Here we use a Gatan heating holder with a tantalum furnace to heat the specimen in TEM. In order to correlate the temperature in *in situ* TEM experiments with those during dielectric measurements on bulk specimens, TEM experiments are first carried out on the single phase BNBT6 (Fig. 2), of which the T_d has been determined to be 115 °C from the dielectric measurement. It has been shown that ~40% of the grains in BNBT6 display a core-shell structure where the core contains micron-sized domains and the shell is filled with nanosized domains [Fig. 2(a)] [19]. The crystal symmetry of the core and shell can be analyzed using the selected area electron diffraction (SAED). According to previous studies on $(Bi_{1/2}Na_{1/2})TiO_3$ and its solid solutions [11,20,21], superlattice diffraction spots in SAED patterns can be used to identify possible space groups [22]. The $[11\bar{2}]$ zone-axis SAED recorded from the core shows discrete ½{*ooo*} superlattice spots [highlighted by the bright circle in the inset in Fig. 2(a)], indicating the *R3c* phase of the micron-sized domains within the core. In contrast, the SAED [the upper right inset in Fig. 2(a)] from the shell region displays clear ½{*ooe*} superlattice spots, suggesting the

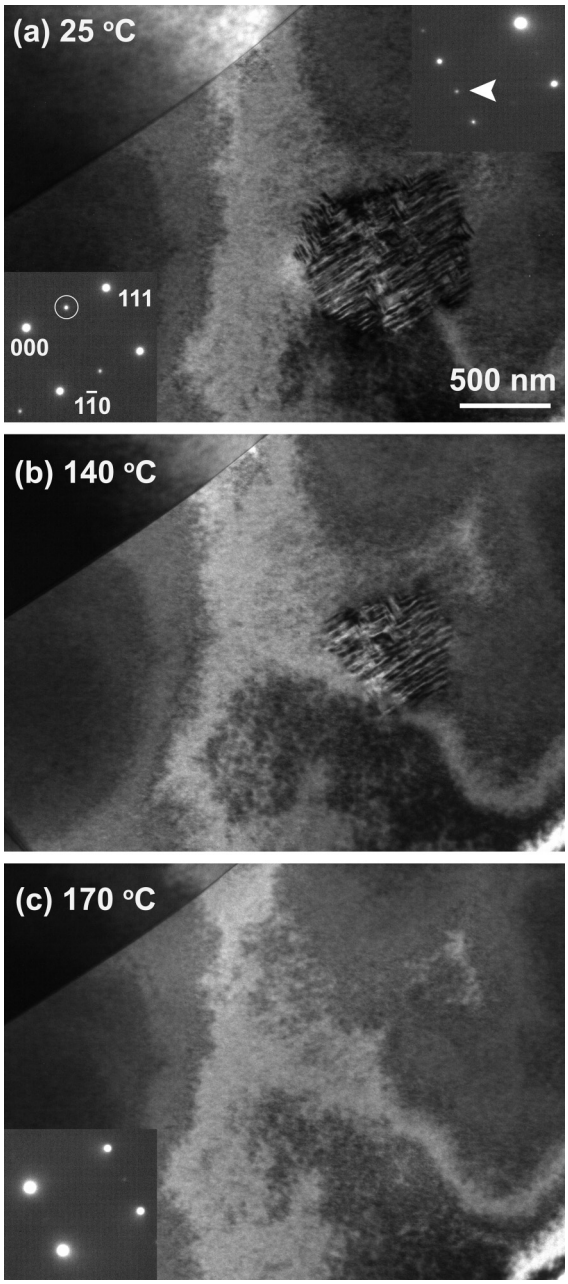

FIG. 2. *In situ* TEM observation of the thermal depolarization in the BNBT6 ceramic. (a) Bright field micrograph of a [$11\bar{2}$] aligned grain with core-shell structure at room temperature. The SAED pattern recorded from the ferroelectric core is displayed in the lower left inset. The ½{*ooo*} superlattice spot is highlighted with the bright circle. The SAED from the shell is displayed in the upper right inset with the ½{*ooe*} superlattice spot indicated with the bright arrow. The same area at (b) 140 °C, and (c) 170 °C. The inset in (c) is the SAED pattern recorded from the same position as in (a).

possible *P4bm* symmetry of the nanosized domains. As the specimen is heated up to 140 °C, the core starts to shrink in volume [Fig. 2(b)]. At 170 °C, the core has been completely replaced by nanosized domains and the SAED pattern recorded from the same position no longer shows the ½{*ooo*} superlattice spots [Fig. 2(c)]. It can be concluded that, first, temperature discrepancy exists between the *in situ* heating TEM experiment and the dielectric measurement on bulk specimens; second, the thermal depolarization in single phase BNBT6 occurs within such a narrow temperature window that corresponds well to the raised plateau in the tanδ curve in Fig. 1(b).

To prepare for the *in situ* heating TEM experiments on the BNBT6/0.3ZnO composite, we first analyze its representative microstructure (Fig. 3). There are three distinguishable phases from the contrast in the scanning electron microscopy (SEM) backscattered electrons micrograph: the bright matrix phase, the grey secondary phase, and the dark secondary phase [Fig. 3(a)]. The element distribution mapping recorded from the same area reveals that the matrix phase is BNBT6; the grey secondary phase contains only Zn and O, while the dark secondary phase contains Zn, Ti, and O. A close examination of the three phases is conducted with TEM. Figure 3(b) displays the annular bright-field scanning transmission electron microscopy (ABF-STEM) image of the BNBT6 matrix viewed along its [001] zone axis. The sites occupied by Bi (Na, Ba), Ti, and O atoms are, respectively, highlighted with purple, green, and blue dots. Figures 3(c) and 3(d) show the morphology of the two types of Zn-containing secondary phases. Even though indistinguishable in the bright field contrast, the two secondary phases are determined to be ZnO [Fig. 3(c)] and Zn_2TiO_4 [Fig. 3(d)] based on the corresponding energy-dispersive spectrum (EDS) displayed in Figs. 3(c_1) and 3(d_1). Interestingly, the microstructure of BNBT6 is altered by forming the composite. As shown in Fig. 2(a), single phase BNBT6 is dominantly occupied with nanosized domains with minor amounts of micron-sized domains in the central portion of some grains [11]. On the contrary, in BNBT6/0.3ZnO, a great number of micron-sized domains exist in BNBT6 grains close to the particle/matrix interface. It was found that the regions occupied by micron-sized domains vary in volume, some are confined in a narrow zone along the interface [Fig. 3(c)], while others can expand deep into the grain interior [Fig. 3(d)]. It should be noted that there seems to be no correlation between the size of the region of micron-sized domains and the type of the secondary phase (ZnO or Zn_2TiO_4).

Then *in situ* heating TEM experiments are conducted on the BNBT6/0.3ZnO composite to reveal the thermal depolarization process. A grain with a large region of micron-sized domains in the BNBT6 matrix is observed along the [$\bar{1}$10] zone axis during heating (Fig. 4). At room temperature, the BNBT6 grain is filled with micron-sized domains, and the ZnO particle resides at the grain boundary triple junction [Fig. 4(a)]. The presence of the ½{*ooo*} superlattice spot, marked by the bright circle on the SAED pattern in the inset, indicates the *R3c* crystal symmetry of the micron-sized domains [11]. When the specimen is heated up in TEM, the domain morphology remains unchanged until 150 °C, when the micron-sized domains start to be replaced by nanosized domains from the left edge of the observed area [Fig. 4(b)]. According to the results shown in Fig. 2, these nanosized domains are of *P4bm* symmetry. At 170 °C, the micron-sized domains in the top left part completely disappear [Fig. 4(c)]. As temperature reaches 190 °C, the micron-sized domains near the bottom edge of the observed area transform into nanosized domains [Fig. 4(d)]. At 210 °C, the volume occupied by micron-sized domains continues to shrink [Fig. 4(e)].

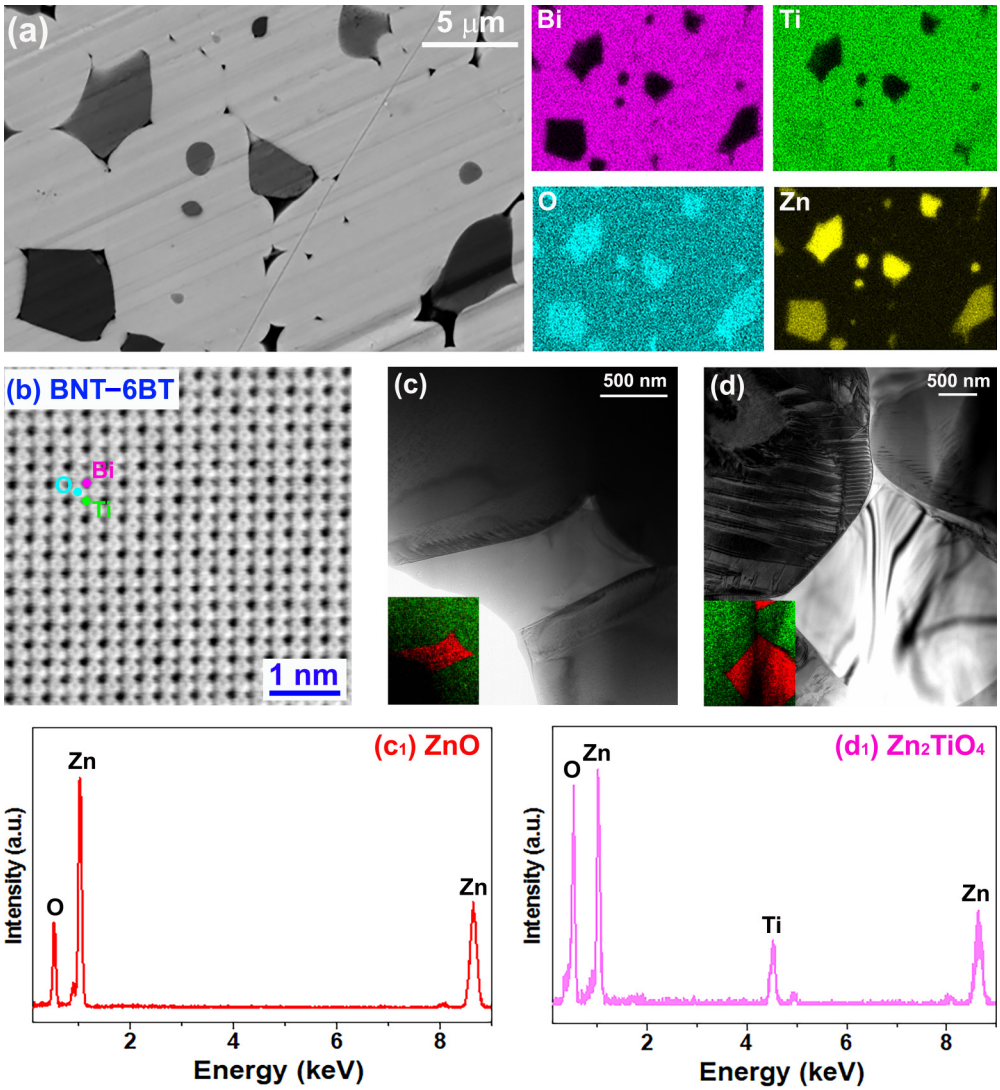

FIG. 3. (a) SEM backscattered electrons image of the overall microstructure of the BNBT6/0.3ZnO composite and the corresponding EDS element maps. (b) ABF-STEM image of the BNBT6 matrix viewed along its [001] zone axis. Bi (Na, Ba), Ti, and O atom columns are marked with colored dots. (c) TEM bright field image of the domain morphology around a ZnO particle [EDS pattern shown in (c_1)]. (d) TEM bright field image of the domain morphology around a Zn_2TiO_4 particle [EDS pattern shown in d_1]. Insets of (c) and (d) show the corresponding EDS mapping of Bi (green) and Zn (red).

At 220 °C, only a few micron-sized domains can be seen in the vicinity of the interface [Fig. 4(f)]. Eventually, the observed area is entirely free of micron-sized domains at 240 °C [Fig. 4(g)]. In the meantime, the ½{*ooo*} superlattice spot in the corresponding SAED pattern shown in the inset disappears. It can be easily derived from the *in situ* heating TEM experiment that the thermal depolarization in the BNBT6/0.3ZnO composite starts at a temperature more or less the same as single phase BNBT6, so T_d is not delayed. Instead, the thermal depolarization process is found to become gradual and spreads over a temperature range spanning approximately 90 °C, much broader than that in the single phase BNBT6. Moreover, the thermal depolarization in BNBT6/0.3ZnO seems to follow a spatial sequence. The micron-sized domains in the BNBT6 grain interior depolarize and disappear first, while those closer to the ZnO particle are able to survive at higher temperatures and depolarize later.

The spatially sequenced thermal depolarization process in BNBT6/0.3ZnO is confirmed in another [$\bar{1}$10] aligned BNBT6 grain (Fig. 5). The grain of interest is again filled with micron-sized domains at room temperature [Fig. 5(a)]. When the temperature increases, the thermal depolarization starts at 117 °C [Fig. 5(b)]. At 137 °C, the micron-sized domains in the left portion completely disappear [Fig. 5(c)]. As the temperature reaches 181 °C, the central portion of the BNBT6 grain becomes free of micron-sized domains [Fig. 5(d)]. At 230 °C, no micron-sized domains are observable except for a few residuals near the ZnO/matrix interface [highlighted by the yellow circle in Fig. 5(e)]. These lamellar domains do not vanish until 271 °C, above which the BNBT6 grain is completely occupied by nanosized domains [Fig. 5(f)]. In this particular grain, the thermal depolarization process takes more than 150 °C (from 117 to 271 °C) to complete. Similar to Fig. 4, the disappearance of micron-sized domains follows

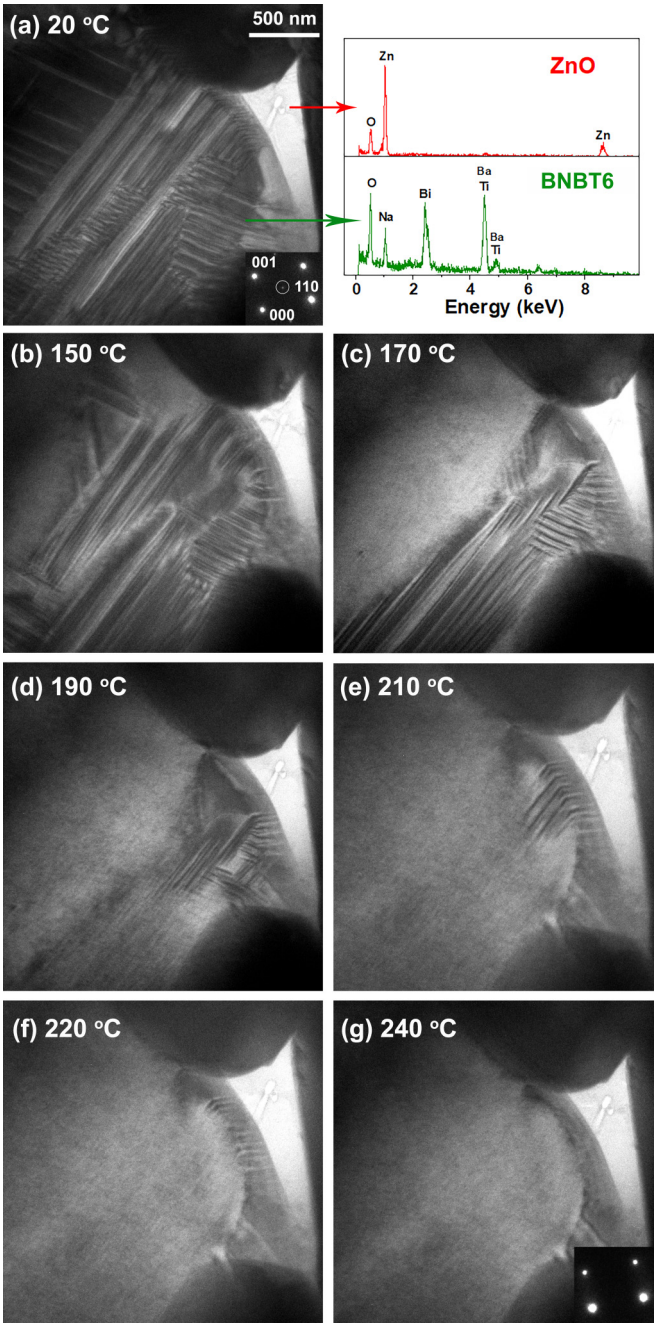

FIG. 4. *In situ* TEM observation of the diffused thermal depolarization in the BNBT6/0.3ZnO composite. The composition is verified with EDS analysis. Bright field images of the domain morphology in a [$\bar{1}$10] aligned BNBT6 grain around a ZnO particle at (a) 25 °C, (b) 150 °C, (c) 170 °C, (d) 190 °C, (e) 210 °C, (f) 220 °C, and (g) 240 °C. The SAED patterns are displayed as insets in (a) and (g). The ½{*ooo*} superlattice spot is highlighted with the bright circle in (a).

the unambiguous spatial sequence, from the region away from the ZnO particle towards the region in contact with the ZnO particle.

B. Impact of ZnO on the diffused thermal depolarization

The introduction of ZnO particles as a secondary phase indeed makes the thermal depolarization in a BNBT6 matrix

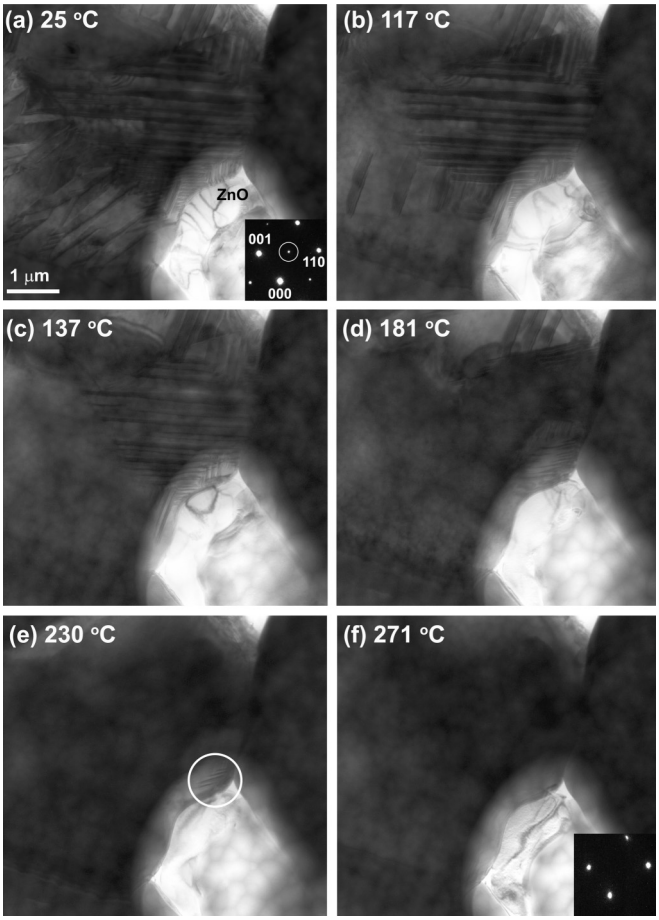

FIG. 5. *In situ* TEM observation of the diffused thermal depolarization in another specimen of the BNBT6/0.3ZnO composite. Bright field images of the domain morphology in another [$\bar{1}$10] aligned BNBT6 grain around a ZnO particle at (a) 25 °C, (b) 117 °C, (c) 137 °C, (d) 181 °C, (e) 230 °C, and (f) 271 °C. The white circle in (e) surrounds the preserved micron-sized domains close to the interface. The SAED patterns are displayed as insets in (a) and (f). The ½{*ooo*} superlattice spot is highlighted with the bright circle in (a).

diffused over a much broader temperature range. More importantly, the ZnO particles seem to have a pinning action to the micron-sized domains and, understandably, the "pinning force" must be stronger at the position closer to them. As a result, the weakly pinned micron-sized domains away from ZnO particles depolarize earlier and those in the region in contact with ZnO particles, which are strongly pinned, remain polarized until much higher temperatures. This is basically in agreement with our "space charge" model proposed in our original report [13]. However, there are still two critical questions to be answered. First, is there evidence to support the "stress field" and the "Zn doping" models? Second, what is the nature of the "pinning force" provided by ZnO particles?

1. "Stress field" model

The interface mismatch strain in ferroelectric thin films has been proved capable of enhancing ferroelectricity in $BaTiO_3$ [23]. A similar effect can even create ferroelectricity at room

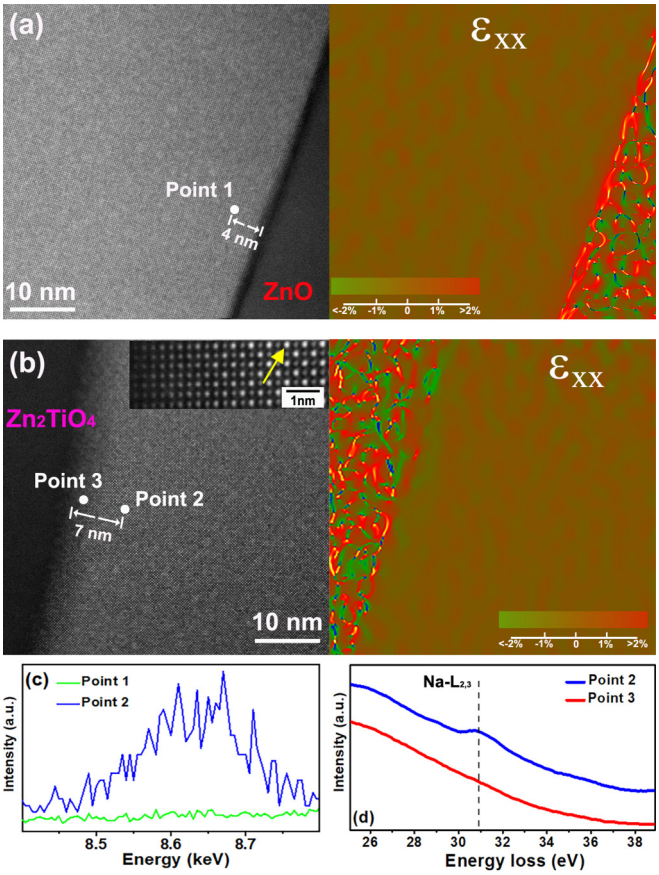

FIG. 6. HAADF-STEM micrographs of BNBT6 grains along their [001] zone axis in contact with a (a) ZnO, and (b) Zn_2TiO_4 particle. Corresponding GPA mapping of the in-plane strain (ε_{xx}) is displayed to the right of each micrograph. The inset in (b) shows the zoomed-in HAADF-STEM image of the BNBT6 grain close to the interface, in which the yellow arrow points at one of the A-site columns. (c) The Zn K-line extracted from the EDS recorded from *Point 1* in (a) and *Point 2* in (b). (d) The Na L-edge extracted from the EELS recorded from *Point 2* and *Point 3* in (b).

temperature in an originally nonpolar $SrTiO_3$ thin film [24]. In the BNBT6/0.3ZnO composite, according to Riemer *et al.* [14], a compressive stress in the BNBT6 matrix results from its higher thermal expansion coefficient than ZnO particles during the cooling process from the sintering temperature. Recently, a compressive stress induced relaxor (pseudocubic) $\rightarrow$ ferroelectric (*R3c* + *P4mm*) phase transition is observed in the BNBT6 bulk ceramic through systematic dielectric and x-ray diffraction studies [25]. Accordingly, the "stress field" model claims that micron-sized ferroelectric domains are formed in the BNBT6 matrix through a stress-induced phase transition [14].

In order to find evidence for the "stress field" model, the strain field in the BNBT6 matrix grain was analyzed. Geometric phase analysis (GPA) is a powerful image-based strain measurement method used in high-resolution STEM micrographs. The basic idea is to calculate and illustrate the deviation of a real local lattice with respect to a reference lattice generated from the electron diffraction pattern [26]. Figures 6(a) and 6(b) display the high-angle annular dark-field scanning transmission microscopy (HAADF-STEM) images of the BNBT6 matrix in contact with ZnO and Zn_2TiO_4 particles, respectively, both of which are viewed along the [001] zone axis. The GPA results (in-plane strain, ε_{xx}) are shown to the right of each HAADF-STEM image. It should be noted that the color contrast of strain mapping in the ZnO and the Zn_2TiO_4 particle do not represent the real strain there because the reference lattice used for GPA is also BNBT6 rather than ZnO or Zn_2TiO_4. In BNBT6, the strain values are uniformly below 1% across the examined area. Similar results are obtained in ε_{yy} (out-of-plane) and ε_{xy} (shear strain) mapping as well. It was shown previously that strains of $<1\%$ can have a significant impact on the ferroelectric phase transitions [27,28]. Therefore, our GPA results seem not able to rule out the stress effect from contributing to the diffused thermal depolarization in the BNBT6/0.3ZnO composite.

2. *"Zn doping" model*

Replacement of Ti^{4+} by Zn^{2+} on the B site of perovskite is likely to strengthen the dipole moment in BO_6 octahedra, and it stabilizes the long-range ferroelectric order in BNBT6 at room temperature [29,30]. The enhanced ferroelectric order can be a direct result of the strong tendency of Zn^{2+} off-center displacement in BO_6 octahedra. In addition, Zn^{2+} is an acceptor dopant for Ti^{4+} on the B site, which can be compensated by oxygen vacancies. Therefore, $(Zn''_{Ti} - V^{\cdot\cdot}_{O})$ defect dipoles are likely to be formed. It has been shown that other acceptor dopants, such as Fe^{3+} and Cu^{2+}, harden the ferroelectric behavior in $(Bi_{1/2}Na_{1/2})TiO_3$-based ceramics and influence their thermal depolarization [31,32]. Accordingly, Mahajan *et al.* attributed the higher T_d in their BNBT6/ZnO composites to the diffusion of Zn into the lattice of BNBT6 matrix, namely the "Zn doping" model [15]. During the sintering process of composite materials, the interdiffusion between different phases is certainly possible. So Zn doping probably also occurs in our BNBT6/0.3ZnO composite. However, when reviewing the works which support the "Zn doping" model, we notice that the thermal depolarization anomaly at T_d in dielectric permittivity vs temperature plots is still observable in BNBT6/ZnO composites, but is consistently $\sim$30 °C higher than the single phase BNBT6 [15,29,33]. So, the diffused thermal depolarization which causes the absence of that particular anomaly in our dielectric measurement cannot be solely attributed to Zn doping.

In order to obtain the exact picture of Zn distribution in the BNBT6 matrix, careful element analysis is conducted. Two points close to the interface are selected in Figs. 6(a) and 6(b), of which *Point 1* is located 4 nm from the ZnO/matrix interface and *Point 2* has a 7-nm distance to the Zn_2TiO_4/matrix interface. The EDS patterns collected from the two points are shown for comparison in Fig. 6(c). Since the Zn L-line overlaps with the Na K-line, only the Zn K-line is displayed for illustration. It can be clearly seen that there is no Zn at *Point 1*, while Zn does exist at *Point 2*. Since the ZnO nanoparticle is the raw material used in the composite processing, it can be seen that there is barely any Zn diffusion from ZnO into the BNBT6 lattice during the sintering. This might be due to the relatively low sintering temperature and the fast heating/cooling rate. On the other hand, Zn_2TiO_4 is very likely

formed through the reaction between ZnO and BNBT6 at high temperatures [34]. The reaction can be expressed as follows (using BNT to represent BNBT6):

$$8ZnO + 4(Bi_{1/2}Na_{1/2})TiO_3 \rightarrow 4Zn_2TiO_4 + Bi_2O_3 + Na_2O. \quad (1)$$

This is supported by further element analysis in the vicinity of Zn_2TiO_4/matrix interface. Since Na and Zn are hard to distinguish in EDS, electron energy-loss spectroscopy (EELS) is employed for Na detection. As shown in Fig. 6(d), the Na L-edge is seen at *Point 2* as expected, but is absent at *Point 3* which is <2 nm away from the interface, implying the existence of a Na deficiency layer in the BNBT6 matrix along the Zn_2TiO_4/matrix interface. Additional EDS analysis on Bi also indicates an even thicker Bi deficiency layer close to the interface. Such an A-site cation deficiency layer can be directly observed in the zoomed-in HAADF-STEM image of the BNBT6 matrix, in which the A-site columns [shown by the yellow arrow in the inset of Fig. 6(b)] become apparently dimmer at the interface (left side). Because Na and Bi are volatile elements, BNBT6 might have lost some Na/Bi at elevated temperatures. After BNBT6 becomes deficient in Na/Bi, the reaction between ZnO and BNBT6 [shown in Eq. (1)] might be promoted, producing Zn_2TiO_4. Other products of this reaction, Bi_2O_3 ($T_m = 817\,°C$) and Na_2O ($T_m = 1132\,°C$), might then be evaporated during sintering. Thus, there exists a Na/Bi deficiency layer at the interface but no Bi_2O_3 or Na_2O segregation is found.

As can be concluded from the above EDS and EELS results, the ZnO nanoparticles in the raw mixture of the composite can be divided into two groups, the first group simply agglomerates into large particles, while the second group reacts with BNBT6. The fact that Zn is only detected in BNBT6 near Zn_2TiO_4 reflects that Zn doping into BNBT6 lattice is accomplished during the reaction (1), rather than the direct diffusion of ZnO into the BNBT6 lattice as was claimed in previous work. In other words, the second group of the ZnO nanoparticles can be regarded as the Zn source, leading to an increase in T_d of the BNBT6 matrix. Even though the magnitude of this increase is moderate, e.g. ~30 °C, the reduced thermal disturbance to the dipole alignment can still provide a large chance for the long-range ferroelectric order in micron-sized domains to form out of the nanosized domains at room temperature [35].

3. *Pinning effect of the ZnO particles*

As discussed in the last section, micron-sized domains occupy a larger volume fraction in BNBT6 grains in the BNBT6/0.3ZnO composite at room temperature than those in the single phase BNBT6 because of Zn doping via reaction (1). Nevertheless, such an effect is not able to render the thermal depolarization gradual and diffused, which is exactly how the BNBT6/0.3ZnO composite behaves. It becomes clear below that the group of ZnO nanoparticles that do not participate in the chemical reaction (1) play a critical role.

When we originally proposed the pinning effect from ZnO using the "space charge" model [13], there was a sufficient condition of DC field poling. The poling field not only induces the micron-sized domains in the BNBT6 matrix, but also

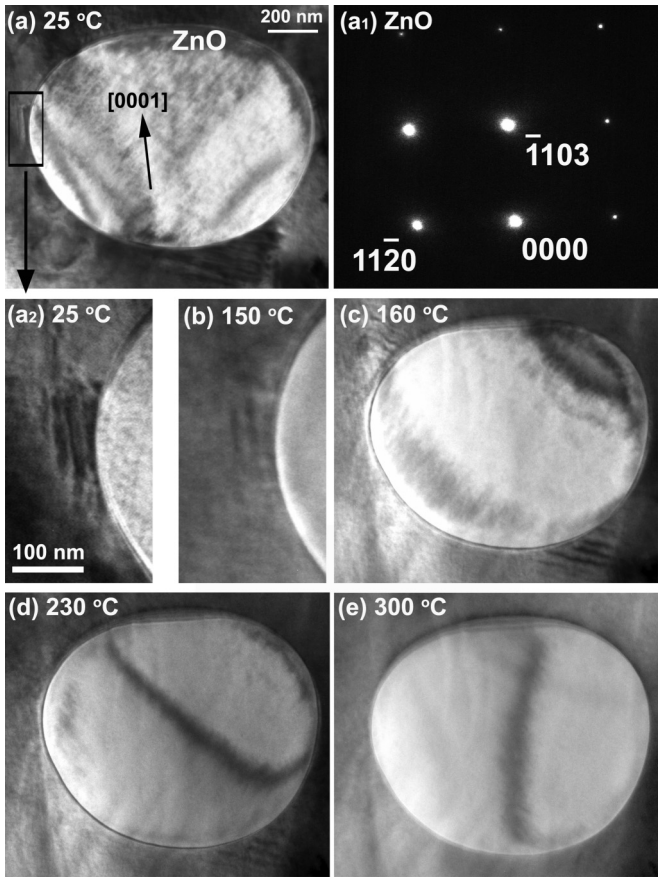

FIG. 7. The anisotropy of the "pinning effect" from a ZnO particle embedded in a BNBT6 grain. (a) Bright field image of two clusters of micron-sized domains around a [3$\bar{3}$02] aligned ZnO particle at (a) 25 °C, (c) 160 °C, (d) 230 °C, and (e) 300 °C. The corresponding SAED pattern recorded from the ZnO particle is shown in (a_1). (a_2) and (b) display the close-up views of the domain cluster in the left at 25 and 150 °C, respectively.

the redistribution of the charges in the semiconductor ZnO at the ZnO/matrix interface. Those charges compensate the depolarization field within the micron-sized domains across the interface, so their transition back into nanosized domains during temperature increase is suppressed. It is well known that ZnO with the wurtzite structure possesses a spontaneous polarization along the polar [0001] axis [36–38]. This provides bound charges along the ZnO/matrix interface even without any externally applied field. This explains why the pinning effect can be clearly observed during our *in situ* heating TEM experiments conducted on unpoled specimens (Figs. 4 and 5).

Since the pinning force stems from the spontaneous polarization in ZnO, it should be highly anisotropic. In other word, the "space charge" model can be indirectly proven if the anisotropy in the pinning effect is verified. For this purpose, a circular shaped ZnO particle with a diameter of ~1 μm is deliberately chosen to be viewed along its [3$\bar{3}$02] zone axis during another *in situ* heating TEM experiment (Fig. 7). The polar [0001] direction in ZnO is projected onto the micrograph plane and marked by the red arrow in Fig. 7(a). The projection angle is 31.7° [Fig. 7(a_1)]. At room temperature, two clusters

of micron-sized domains are present in the BNBT6 matrix, respectively, located close to the lower [Fig. 7(a)] and the left part of the ZnO inclusion [Fig. 7(a_2)]. From room temperature to 150 °C, neither of the two clusters of domains depolarize [Fig. 7(b)]. At 160 °C, the domains close to the left side of the ZnO inclusion disappear while the other domains close to the lower side of ZnO persist [Fig. 7(c)]. When the temperature reaches 230 °C, the straight domain walls are still observable in that particular region close to the lower side of ZnO [Fig. 7(d)]. As the specimen is further heated up to 300 °C, all the micron-sized domains disappear [Fig. 7(e)]. It should be noted that the changes in the contrast and shape of the ZnO particle in Fig. 7 is due to the slight adjustment of tilting to optimize the domain contrast in the BNBT6 matrix; therefore, they do not reflect real changes of the ZnO particle in this temperature range.

These two clusters of micron-sized domains are very likely formed due to the same reasons as for the ferroelectric core in Fig. 2. The domains close to the left side of the ZnO inclusion disappear at the temperature almost the same as for the ferroelectric core in Fig. 2(b) and for the domains far away from the ZnO particles in Figs. 4(b) and 5(b). It indicates that despite the very short distance, the domains close to the left side of the ZnO inclusion do not receive any pinning force from ZnO at all. On the contrary, the domains close to the lower side of the ZnO inclusion are indeed pinned up to the temperature that is roughly the same as the final stage of the diffused thermal depolarization process [Figs. 4(f) and 5(e)]. It should be noted that the projected direction of the polar [0001] axis of ZnO exactly points to this set of micron-sized domains [Fig. 7(a)]. Therefore, the anisotropy in the pinning effect is experimentally verified in Fig. 7 and is further schematically illustrated in Fig. 8. The 2D diagram can be regarded as the micrograph plane in Fig. 7 after it is tilted for 31.7° to have the [0001] polar axis (bright arrow) in-plane. The polarization in the micron-sized domains in the BNBT6 matrix are drawn in accordance with the most common configuration in rhombohedral ferroelectric crystals. The positive and negative charges are separated along the [0001] polar axis and, respectively, bound at the bottom and top ZnO/matrix interface. On the other hand, there is no spontaneous polarization along the direction perpendicular to [0001] in ZnO. Therefore, there are no bound charges at the left or right side of the ZnO/matrix interface. As a result, the domains located close to the bottom interface are pinned by the bound charges but the domains in contact with the left interface have no chance to receive any pinning force. When the temperature is above T_d, the unpinned domains in the left side disappear while the pinned ones close to the bottom interface persist. Such an anisotropy in the pinning effect strongly supports our original "space charge" model and further indicates that the spontaneous polarization of ZnO is the source of pinning charges.

However, there are several points that need to be made clear. First, the presence of spontaneous polarization in ZnO seems not sufficient to trigger the formation of micron-sized domains, but is sufficient to stabilize the already formed micron-sized domains. This explains the fact that there are no micron-sized domains close to the top ZnO/matrix interface, even though there exist bond charges from the spontaneous

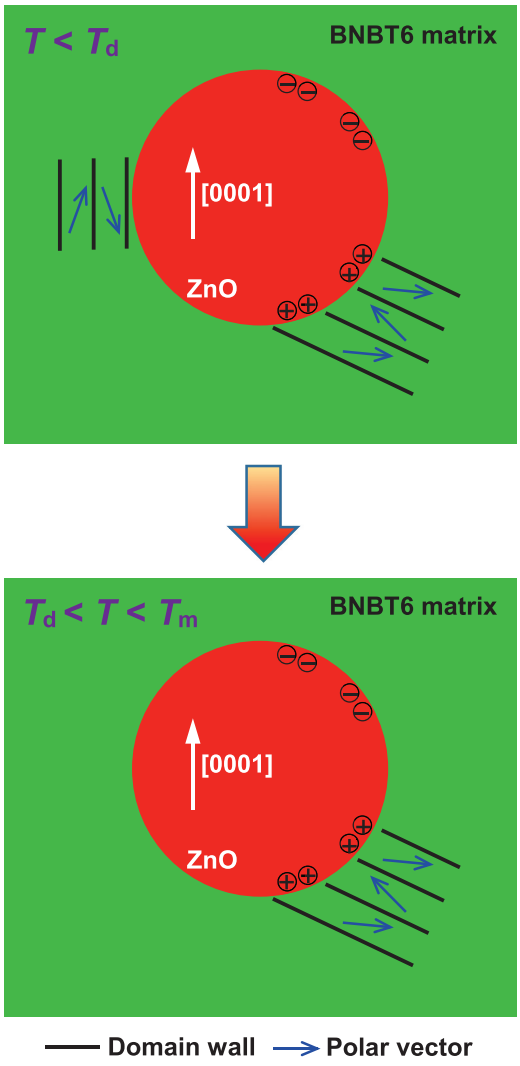

FIG. 8. Schematic illustration of the anisotropic pinning effect from a ZnO particle on the lamellar ferroelectric domains in the BNBT6 matrix. The upper panel depicts the situation at temperatures below T_d while the lower panel illustrates the situation at temperatures between T_d and T_m. The polar [0001] direction of ZnO is marked with the bright arrow.

polarization of the ZnO inclusion. These bond charges, however, are capable of stabilizing the existing micron-sized domains close to the bottom interface. Second, since our GPA results do not rule out the "stress field" model, there could be tensile stresses in the ZnO inclusion to balance the compressive stresses in the BNBT6 matrix [14]. Through the piezoelectric effect of ZnO, such residual stresses are expected to increase the bound charges at the ZnO/matrix interface, which in turn will strengthen the "pinning effect" on the micron-sized domains. Third, even though the model shown in Fig. 8 is plausible, we admit it is an oversimplified illustration and ignores some details. For example, the polarization directions of those lamellar domains are not experimentally determined and there are segments on the BNBT6/ZnO interface with the "head-to-head" polarization configuration. Further studies are still needed to improve the model.

IV. CONCLUSIONS

In summary, extensive TEM experiments are conducted to reveal the mechanisms of the thermal depolarization in the BNBT6/0.3ZnO composite. *In situ* heating TEM indicates that the thermal depolarization in the composite is not just simply shifted to higher temperatures, rather it becomes gradual and diffused. GPA results suggest a strain field of magnitude $<1\%$ is present in the BNBT6 matrix. Combined EDS and EELS analysis indicate that the existence of a high volume fraction of micron-sized ferroelectric domains in BNBT6 grains in the composite at room temperature is likely due to Zn doping into the BNBT6 perovskite lattice, which is accomplished through the chemical reaction between ZnO and BNBT6. Once the micron-sized domains are formed in the BNBT6 grain, they are pinned by the charges in ZnO originating from its spontaneous polarization. Correspondingly, the pinning effect displays a strong anisotropy with respect to the [0001] polar axis of ZnO. It is observed that the thermal depolarization process in the BNBT6 matrix starts from positions farther away from ZnO and gradually progresses to the ZnO/BNBT6 interface, a continuous process spanning over a wide temperature range of more than 100 °C.

ACKNOWLEDGMENTS

This work was supported by the National Science Foundation (NSF) through Grant No. DMR-1465254 and Laboratory Directed Research and Development funds at the US Department of Energy (DOE) Ames Laboratory (T.-H.K. and L.Z.). All electron microscopy work was performed at the Sensitive Instrument Facility at Ames Laboratory, which is operated for the US DOE by Iowa State University under Contract No. DE-AC02-07CH11358. J.Z. and S.-T.Z. acknowledge the financial support from the National Nature Science Foundation of China (11674156).

[1] Y. Saito, H. Takao, T. Tani, T. Nonoyama, K. Takatori, T. Homma, T. Nagaya, and M. Nakamura, Nature (London) **432**, 84 (2004).
[2] J. Rödel, W. Jo, K. T. Seifert, E. M. Anton, T. Granzow, and D. Damjanovic, J. Am. Ceram. Soc. **92**, 1153 (2009).
[3] W. Liu and X. Ren, Phys. Rev. Lett. **103**, 257602 (2009).
[4] M. Acosta, N. Novak, V. Rojas, S. Patel, R. Vaish, J. Koruza, G. A. Rossetti, and J. Rödel, Appl. Phys. Rev. **4**, 041305 (2017).
[5] Z. Fan, J. Koruza, J. Rödel and X. Tan, Acta Mater. **151**, 253 (2018).
[6] J. Wu, D. Xiao, and J. Zhu, Chem. Rev. **115**, 2559 (2015).
[7] A. M. Mazuera, P. S. Silva, A. D. Rodrigues, P. S. Pizani, Y. Romaguera-Barcelay, and M. Alguero, Phys. Rev. B **94**, 184101 (2016).
[8] S. Körbel, P. Marton, and C. Elsässer, Phys. Rev. B **81**, 174115 (2010).
[9] X. Liu and X. Tan, Adv. Mater. **28**, 574 (2016).
[10] M. Vögler, N. Novak, F. H. Schader, and J. Rödel, Phys. Rev. B **95**, 024104 (2017).
[11] C. Ma, X. Tan, E. Dul'kin, and M. Roth, J. Appl. Phys. **108**, 104105 (2010).
[12] C. Ma, H. Guo, and X. Tan, Adv. Funct. Mater. **23**, 5261 (2013).
[13] J. Zhang, Z. Pan, F. F. Guo, W. C. Liu, H. Ning, Y. B. Chen, M. H. Lu, B. Yang, J. Chen, S. T. Zhang, X. Xing, J. Rödel, W. Cao, and Y. F. Chen, Nat. Commun. **6**, 6615 (2015).
[14] L. M. Riemer, K. V. Lalitha, X. Jiang, N. Liu, C. Dietz, R. W. Stark, P. B. Groszewicz, G. Buntkowsky, J. Chen, S. T. Zhang, J. Rödel, and J. Koruza, Acta Mater. **136**, 271 (2017).
[15] A. Mahajan, H. Zhang, J. Wu, E. V. Ramana, M. J. Reece, and H. Yan, J. Phys. Chem. C **121**, 5709 (2017).
[16] E. M. Anton, W. Jo, D. Damjanovic, and J. Rödel, J. Appl. Phys. **110**, 094108 (2011).
[17] A. A. Bokov and Z.-G. Ye, J. Mater. Sci. **41**, 31 (2006).
[18] C. W. Tai, S. H. Choy, and H. L. W. Chan, J. Am. Ceram. Soc. **91**, 3335 (2008).
[19] C. Ma and X. Tan, J. Am. Ceram. Soc. **94**, 4040 (2011).
[20] G. O. Jones and P. A. Thomas, Acta Cryst. B **58**, 168 (2002).
[21] J. Petzelt, S. Kamba, J. Fábry, D. Noujni, V. Porokhonskyy, A. Pashkin, I. Franke, K. Roleder, J. Suchanicz, R. Klein, and G. E. Kugel, J. Phys. Condens. Matter **16**, 2719 (2004).
[22] D. I. Woodward and I. M. Reaney, Acta Cryst. B **61**, 387 (2005).
[23] K. J. Choi, M. Biegalski, Y. L. Li, A. Sharan, J. Schubert, R. Uecker, P. Reiche, Y. B. Chen, X. Q. Pan, V. Gopalan, L. Q. Chen, D. G. Schlom, and C. B. Eom, Science **306**, 1005 (2004).
[24] J. H. Haeni, P. Irvin, W. Chang, R. Uecker, P. Reiche, Y. L. Li, S. Choudhury, W. Tian, M. E. Hawley, B. Craigo, A. K. Tagantsev, X. Q. Pan, S. K. Streiffer, L. Q. Chen, S. W. Kirchoefer, J. Levy, and D. G. Schlom, Nature (London) **430**, 758 (2004).
[25] F. H. Schader, Z. Wang, M. Hinterstein, J. E. Daniels, and K. G. Webber, Phys. Rev. B **93**, 134111 (2016).
[26] Y. Zhu, C. Ophus, J. Ciston, and H. Wang, Acta Mater. **61**, 5646 (2013).
[27] L. Zhang, Y. Yuan, J. Lapano, M. Brahlek, S. Lei, B. Kabius, V. Gopalan, and R. Engel-Herbert, ACS Nano **12**, 1306 (2018).
[28] C. H. Lee, V. Skoromets, M. D. Biegalski, S. Lei, R. Haislmaiser, M Bernhagen, R. Uecker, X. Xi, V. Gopalan, X. Marti, S. Kamba, P. Kužel, and D. G. Schlom, Appl. Phys. Lett. **102**, 082905 (2013).
[29] L. Li, M. Zhu, K. Zhou, Q. Wei, M. Zheng, and Y. Hou, J. Appl. Phys. **122**, 204104 (2017).
[30] I. Grinberg, M. R. Suchomei, P. K. Davies, and A. M. Rappe, J. Appl. Phys. **98**, 094111 (2005).
[31] E. Aksel, E. Erdem, P. Jakes, J. L. Jones, R. A. Eichel, Appl. Phys. Lett. **97**, 012903 (2010).
[32] W. Jo, J.-B. Ollagnier, J.-L. Park, E.-M. Anton, O.-J. Kwon, C. Park, H.-H. Seo, J.-S. Lee, E. Erdem, R. A. Eichel, and J. Rödel, J. Eur. Ceram. Soc. **31**, 2107 (2011).
[33] W. Bai, P. Zheng, F. Wen, J. Zhang, D. Chen, J. Zhai, and Z. Ji, Dalton Trans. **46**, 15340 (2017).
[34] Y. C. Lee, T. K. Lee, and J. H. Jan, J. Eur. Ceram. Soc. **31**, 3145 (2011).
[35] D. Viehland, S. J. Jang, L. E. Cross, and M. Wuttig, J. Appl. Phys. **68**, 2916 (1990).

[36] Ü, Özgür, Y. I. Alivov, C. Liu, A. Teke, M. A. Reshchikov, S. Doğan, V. Avrutin, S. J. Cho, and H. Morkoc, J. Appl. Phys. **98**, 041301 (2005).

[37] J. Zhang, Y. Zhang, K. Tse, and J. Zhu, Phys. Rev. Mater. **2**, 013403 (2018).

[38] T. C. Rödel, J. Dai, F. Fortuna, E. Frantzeskakis, P. Le Fevre, F. Bertran, M. Kobayashi, R. Yukawa, T. Mitsubashi, M. Kitamura, K. Horiba, H. Kumigashira, and A. F. Santander-Syro, Phys. Rev. Mater. **2**, 051601 (2018).